Journal of Power Sources 195 (2010) 4391–4399

Contents lists available at ScienceDirect

Journal of Power Sources

journal homepage: www.elsevier.com/locate/jpowsour

Characterization of equivalent series resistance of electric double-layer capacitor electrodes using transient analysis

Songhun Yoon[a,b,*], Chul Wee Lee[a], Seung M. Oh[b]

[a] Green Chemical Technology Division, Korea Research Institute of Chemical Technology (KRICT), Daejeon 305-600, Republic of Korea
[b] Research Center for Energy Conversion and Storage (RCECS), School of Chemical and Biological Engineering and Institute of Chemical Process, College of Engineering, Seoul National University, Seoul 151-744, Republic of Korea

ARTICLE INFO

Article history:
Received 20 November 2009
Received in revised form
23 December 2009
Accepted 22 January 2010
Available online 10 February 2010

Keywords:
Electric double-layer capacitors
Transient analysis
Equivalent series resistance
Mesoporous carbon
Transmission line model

ABSTRACT

In this study, transient equations based on chronoamperometry (CA), chronopotentiometry (CP), electrochemical impedance spectroscopy (EIS) and imaginary capacitance analysis (ICA) are proposed using two equivalent circuit models for the purpose of accurate estimation of the equivalent series resistance (ESR) in electric double-layer capacitor (EDLC) electrodes. After examining transient equations based on a simple resistance–capacitance series connection, alternative equations with a more complicated form are proposed using the transmission line model. From these equations, it is theoretically predicted that one-third of the electrolyte resistance within the pores contributes to the total ESR, irrespective of the electrochemical analysis method employed. As EDLC electrode materials, mesoporous carbons with different pore structure (size, surface area) are prepared by the direct template method. After fabrication of EDLC electrodes using these materials, transient experiments using CA, CP, EIS, and ICA are conducted, and a consistent ESR is obtained. From ESR comparison, it is observed that the increase in ESR is mostly attributable to the electrolytic resistance in the pores and is highly correlated with the pore structure of the carbon electrodes. Additionally, it is found that a mesoporous carbon electrode with a 2-h reaction time exhibits an improved rate performance comparable with that of ordered mesoporous carbon electrodes prepared by the templating of ordered mesoporous silica.

1. Introduction

Electric double-layer capacitors (EDLCs) have been extensively investigated for use in high-power sources due to their high charge utilization (capacitance) and fast charge storage (rate capability) [1–5]. Generally, porous carbon with a high surface area has been employed as an EDLC electrode material because of the highly available charge storage sites on the pore surfaces [2–4]. In regards to another important EDLC performance factor, the rate capability of EDLC electrodes makes them attractive for high-power applications [4–8]. In particular, the resistance of EDLC electrodes, as represented by the equivalent series resistance (ESR), should be minimized because the rate capability is inversely proportional to the ESR [2–5]. As reported in many studies, the ESR in EDLC electrodes can be expressed by a series connection of all resistance components relevant to charge transfer and electrolyte and electron transport [3–6]. Normally, the charge-transfer reaction of EDLCs is negligible due to their intrinsic charge accumulation, which occurs predominantly in the electric double-layer [3]. Furthermore, the electrode resistance of EDLCs induced by electron transport becomes insignificant because conventional EDLC electrodes employ porous carbon materials with a high electrical conductivity, or a conducting agent, such as carbon black or graphite, is added during fabrication to enhance the electrical conductivity [3,5]. Many studies have revealed that electrolyte resistance is the major contributor to the ESR of EDLC electrodes [2–4,9].

Generally, the electrolyte resistance in EDLC electrodes can be classified into three types of resistance that are related to ion transport in the pores of the porous materials within the electrode layer and in the bulk electrolyte solution. In our previous study [9], these resistances were obtained separately by thickness-dependent imaginary capacitance analysis (ICA) using ordered mesoporous carbon electrodes [9]. The derived equations required exact control of the thickness and a well-defined pore structure to calculate the number of stacked pores in the porous carbon within the electrode. Furthermore, the equations could only be applied for ICA due to the high complexity of the corresponding equivalent circuit [9]. For very thin electrodes, the electrolyte resistance within the electrode layer becomes negligible, and this

* Corresponding author at: Green Chemical Technology Division, Korea Research Institute of Chemical Technology (KRICT), Daejeon 305-600, Republic of Korea. Tel.: +82 42 860 7199; fax: +82 42 860 7388.
E-mail address: yoonshun@krict.re.kr (S. Yoon).

0378-7753/$ – see front matter © 2010 Elsevier B.V. All rights reserved.
doi:10.1016/j.jpowsour.2010.01.086

indicates that the other two resistances are major contributors to the ESR. After excluding the electrolyte resistance within the electrode layer in thin electrodes, the equivalent circuit describing the EDLC electrode was converted into a simple transmission line model (TLM). Although several researchers have employed the TLM for analysis of EDLC electrodes, there have been few studies that employ a systemized approach to the estimation of the ESR using electrochemical transient analysis methods based on the TLM [10–14]. Additionally, the application of derived transient equations to porous electrodes with delicately controlled pores has seldom been attempted. Hence, it is necessary to establish useful transient equations based on the TLM for chronoamperometry (CA), chronopotentiometry (CP), electrochemical impedance spectroscopy (EIS), and ICA to understand the physical meaning of the ESR and to calculate its value accurately.

Hence, the purpose of the present work is to establish a theoretical background and obtain transient equations that are the useful for the estimation of the ESR of EDLC electrodes. To this end, transient equations for CA, CP, EIS, and ICA are proposed based on the TLM. The direct template method is employed for delicate control of the pore structure of the carbon electrodes as it has proven useful in the preparation of mesoporous carbon [5–7,15,16]. As an EDLC electrode material, mesoporous carbon with different pore structures (size, surface area) is prepared by the direct template method. After fabrication of the EDLC electrodes using these materials, transient experiments using CA, EIS, CP and ICA are conducted and the ESR is estimated.

2. Experimental

Several reports in the literature have suggested use of the direct template method for the preparation of mesoporous carbon, and it has been shown that carbon materials prepared by this method exhibit improved EDLC performance [5–7,17]. To synthesize porous carbon in this study, surfactant (cetyltrimethylammonium bromide, CTAB) was dispersed in deionized water, into which tetraethylorthosilicate (TEOS) was added with NaOH. The molar ratio of CTAB:TEOS:NaOH:H_2O was 1:2:1:1100 [18–21]. The solution was stirred at 40 °C for 2–16 h to generate a CTAB/silicate template. In this process, CTAB and silicate are organized into self-assembled silicate micelles (SSM) during the reaction period [20], and it is known that cross-linking between SSMs is strengthened according to reaction time. A separate solution of resorcinol (R) and formaldehyde (F) was prepared with Na_2CO_3 (as a polymerization catalyst) in a molar ratio of R:F:Na_2CO_3:H_2O = 10:20:1:100. The solution was reacted for 0.5 h to produce RF oligomers in solution. Two solutions were mixed at a molar ratio of R:TEOS = 1:1, stirred vigorously, and aged at 85 °C for 1 week. During this period, the silicate was transformed to silica *via* polymerization/condensation and the RF sol was converted into a gel [22]. The resulting precipitate (CTAB + SiO_2 + RF) was filtered, dried in air at 85 °C, and heat-treated at 1000 °C under an argon atmosphere for 1 h to remove CTAB and to carbonize the RF gel. In the final step, silica in the composite was removed by hydrofluoric acid. FE-SEM and TEM images were obtained with JEOL JSM-6700F and JEM-2010 equipment, respectively. The isotherms were collected at 77 K with a Micromeritics ASAP 2020 Gas Adsorption Analyzer.

To prepare the composite electrodes, a mixture of prepared carbon, polytetrafluoroethylene (PTFE, as a binder) and Ketjenblack ECP-600JD (as the carbon additive for conductivity enhancement, 10:1:1 in weight ratio) was dispersed in isopropyl alcohol and coated on a stainless-steel Exmet (apparent area = 2 cm^2) that served as the current-collector [5–7]. The electrode plate was pressed and dried under vacuum at 120 °C for 12 h. To minimize the effect of inter-particle pores, loading of active materials was as small as 2.5 mg cm^{-2} and the measured electrode thickness was approximately 10 μm [9]. The electrode thickness was measured using a micrometer (Mitutoyo Co.).

The chronoamperometry, chronopotentiometry and a.c.-impedance measurements were taken with a three-electrode configuration in 2.0 M H_2SO_4 electrolyte. A platinum flag and a SCE (saturated calomel electrode) were employed as the counter and reference electrode, respectively, and an Ivium® potentiostat was utilized to apply a current step (10 mA), voltage step (10 mV) and a sinusoidal voltage of 10 mV amplitude for a.c.-impedance measurements. The frequency range was 10^6 Hz–5 mHz. The base potential was chosen as 0.2 V to avoid a pseudo-capacitance effect after stabilization below 2 μA at 0.5 V *vs.* SCE. Mathcad 2000 Professional (MathSoft Inc.) software was used for the numerical calculations.

3. Theory

3.1. Simplest equivalent circuit model of EDLC electrodes

Schematic drawings of (a) the EDLC electrode structure and (b) the simplest equivalent circuit describing the EDLC electrode are presented in Fig. 1. In this model, the charge-transfer resistance corresponding to the faradaic reaction is excluded for convenience. Theoretically, the ESR is estimated by simple summation of all resistance components connected in series and appears as a corresponding voltage drop induced by perturbation of the current in the EDLC system [2,3]. In Fig. 1, the ESR components are the electrical resistance of the electrode ($R_{electrode}$), the total electrolyte resistance ($R_{electrolyte}$) and the bulk electrolyte resistance (R_{bulk}); ESR (R) = $R_{electrode}$ + R_{bulk} + $R_{electrolyte}$. Based on this model, the transient equations are given as follows.

When the potential step (V_0) is applied to the electrodes (potentiostatic condition), the following current transient ($I(t)$) with time (t) is given as [23]:

$$I(t) = \frac{V_0}{R} e^{-t/(RC_0)} \quad (1)$$

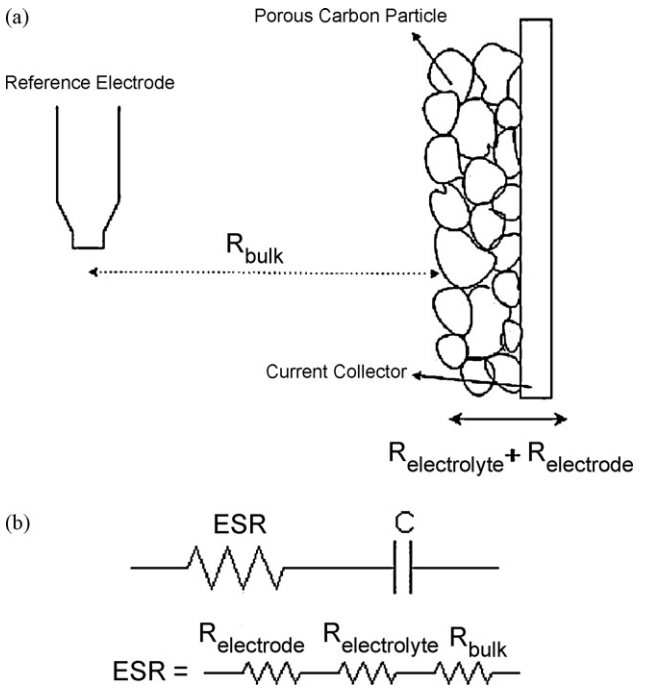

Fig. 1. (a) Schematic drawing of EDLC system to demonstrate resistance component of equivalent series resistance. (b) Simplest equivalent circuit model of EDLC electrodes.

where R and C_0 are the equivalent series resistance (ESR) and capacitance of the electrode, respectively. Hence, in the chronoamperometry (CA) transient experiment, a simple exponential decay is expected for electric double-layer charging [5–7].

In the case where a current step with a magnitude of I_0 is applied (galvanostatic condition), the following describes the corresponding potential transient behaviour ($V(t)$).

$$V(t) = I_0 \left(R + \frac{t}{C_0} \right) \tag{2}$$

As shown in Eq. (2), a potential I_0R, arises initially and, subsequently, a sloped line with increasing time is expected in the chronopotentiometry (CP) transient experiment [23].

In the a.c.-impedance experiment (EIS), the frequency-dependent impedance $Z(f)$ is expressed as [2,3]:

$$Z(f) = R - j\frac{1}{2\pi f C_0} \tag{3}$$

This relationship indicates that a simple vertical straight line should be observed in the Nyquist plot if the EDLC electrodes follow the simplest equivalent circuit model described above in Fig. 1(b). Eqs. (1)–(3) have very simple forms, which make it easy to calculate the ESR and C_0. Therefore, an analysis based on Eqs. (1)–(3) has been used for the characterization of the EDLC electrodes in many studies [5–7].

As shown in Fig. 1(b), however, the equivalent circuit model that is utilized is an oversimplification of the porous electrode system, which is usually composed of narrow and long pores because micro or mesoporous carbon with a high surface area is generally employed as the electrode material [5–7,16]. Hence, a more realistic equivalent circuit should be utilized for the correct description of EDLC electrodes.

3.2. Transmission line model of EDLC electrodes

The transmission line model (TLM) has been proposed by many researchers to describe porous systems more accurately [10–14]. An EDLC electrode using porous carbon is described schematically in Fig. 2. For a very thin electrode, the electrolyte resistance at the inter-particle pores can be disregarded, and the overall intra-particle pores are assumed to be arranged in the form of parallel connections, as shown in Fig. 2(a) [9]. In this figure, a case involving four pores ($m = 4$) within one particle ($n = 1$) is given, and the corresponding equivalent circuit for the electrodes is presented in Fig. 2(b). Here Z_p is the impedance of one pore, and the other notations are identical to those in Fig. 1. For the sake of clarity and mathematical convenience, the influence of $R_{electrode}$ is excluded. According to the transmission line model proposed by de Levie [10], Z_p can be expressed as an equivalent circuit, as shown in Fig. 2(c), and the resulting differential equation for the time (t) and position (y) dependent overpotential ($V(y, t)$) is given as [10,13]:

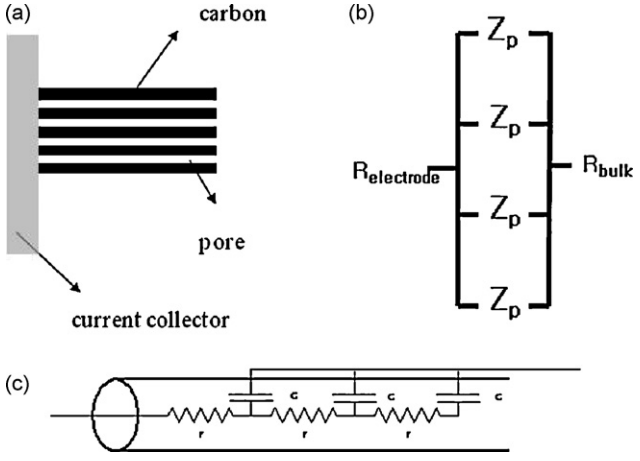

Fig. 2. (a) Schematic illustration of thin electrode. Here, a case of four pores ($m = 4$) within one particle ($n = 1$) is given. (b) Equivalent circuit of (a). (c) Transmission line model describing for one pore (Z_p). The meaning of symbols is separately listed in Appendix A.

$$\frac{\partial^2 V(y,t)}{\partial y^2} = \tau \frac{\partial V(y,t)}{\partial t} \tag{4}$$

where y and τ are dimensionless parameters corresponding to the pore length and time constant, respectively. Additionally, the current can be expressed as [10]:

$$I(t) = -\frac{1}{R_p}\left[\frac{\partial V(y,t)}{\partial y}\right]_{y=0} \tag{5}$$

where R_p is the electrolyte resistance within one pore. Under the assumption of zero initial overpotential and no potential gradient at the end of the pore ($V(y, 0) = V(1, t) = 0$), Z_p is given as Eq. (6) using the Laplace transform of Eqs. (4) and (5) [8–10], i.e.,

$$Z_p(s) = \frac{V(s)}{I(s)} = \frac{R_p}{\sqrt{\tau s}}\coth[\sqrt{\tau s}] \tag{6}$$

where s is a parameter in the Laplace domain. Under the conditions of parallel connection of the overall pores, the total impedance of the electrolyte ($Z(s)$) can be expressed as:

$$Z(s) = \frac{Z_p(s)}{N_p} = \frac{1}{mn}\frac{R_p}{\sqrt{\tau s}}\coth[\sqrt{\tau s}] = \frac{R_t}{\sqrt{\tau s}}\coth[\sqrt{\tau s}] \tag{7}$$

where N_p, n, and R_t are the total number of pores in the electrodes, the number of particles in the porous materials, and the total electrolyte resistance in the pores, respectively. In Fig. 2, one particle with four pores is depicted ($m = 4$, $n = 1$ and $N_p = 4$). Eq. (7) is utilized to obtain the transient equations, which have a different form according to the change in the external fluctuation conditions. From these equations, R_t and ESR are estimated.

First, in the CA experiment, the applied potential step in the Laplace domain is given by:

$$V(s) = \frac{V_0}{s(1 + \rho\sqrt{\tau s})} \tag{8}$$

The resulting current in the Laplace domain is expressed by:

$$I(s) = \frac{V(s)}{Z(s)} = \frac{V_0\sqrt{\tau s}}{sR_t(1 + \rho\sqrt{\tau s})}\tanh\sqrt{\tau s} \tag{9}$$

According to the literature, the inversion of Eq. (9) produces [13]:

$$I(t) = \frac{2V_0}{R_t}\sum_p \frac{\sin(p)\exp(-p^2 t/\tau)}{(1+\rho)\sin(p) + \rho p\cos(p)} \tag{10}$$

where ρ and p are parameters obtained from the relationships, $\rho = R_{bulk}/R_t$ and $p\tan(p) = 1/\rho$, respectively. In Fig. 3(a), the graph showing the relationship between $I(t)R_t/V_0$ *vs.* t/τ under the condition of $R_{bulk} = 0$ is given as a solid line. Additionally, the exponential decay based on Eq. (1) is included as a dotted line for comparison. From this comparison, it can be seen that the difference between the two becomes larger with increasing time, which is indicative of distributed behaviour caused by ionic penetration into the pores. Since it is difficult to find the analytical relationship between Eqs. (1) and (10), the correlation between R_t and $R_{electrolyte}$ will be discussed later. Since Eq. (10) is too complex to use for practical purposes, it should be converted into a simple and useful form. For a tangent line from the zero point, the current is given by [13]:

$$I(t) = \frac{V_0}{\sqrt{\pi}R_t}\left(\frac{\tau}{t}\right)^{0.5} \tag{11}$$

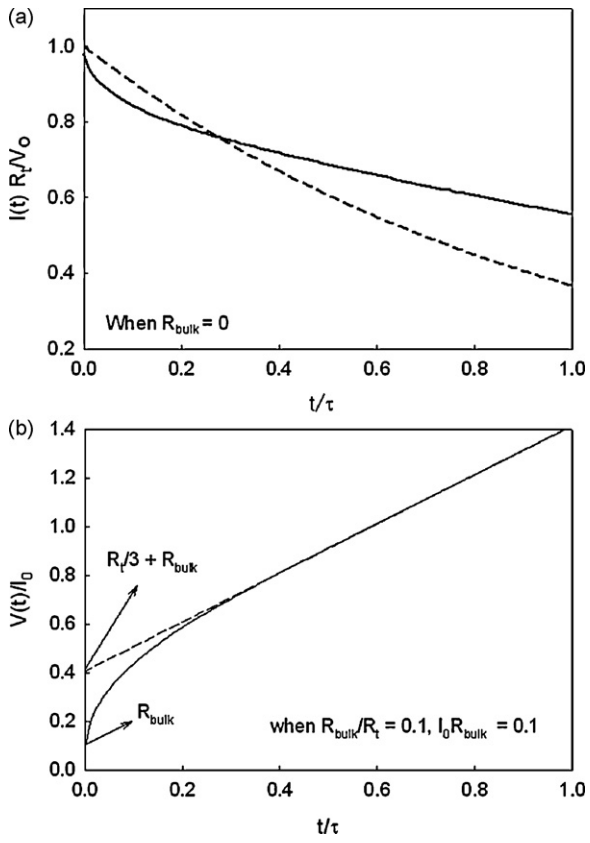

Fig. 3. (a) Typical current transient showing relationship between $I(t)\ R_t/V_0$ *vs.* t/τ when $R_{bulk} = 0$ (solid line). Simple exponential decay is shown as dotted line. (b) Typical potential transient ($V(t)/I_0$) *vs.* t/τ when $R_{bulk}/R_t = 0.1$ and $I_0R_{bulk} = 0.1$ is expressed as solid line. Dotted line describes value of intercept in $V(t)/I_0$ axis of $R_t/3 + R_{bulk}$.

Eq. (11) is utilized to obtain the value of R_t.

For the CP, the resulting equations in the Laplace domain (Eq. (13)) and time domain (Eq. (14)) are given using the external fluctuation condition expressed:

$$I(s) = \frac{I_0}{s} \tag{12}$$

$$V(s) = Z(s) \times I(s) = \frac{I_0 R_t}{s\sqrt{\tau s}} \coth \sqrt{\tau s} \tag{13}$$

$$V(t) = I_0 R_{bulk} + I_0 R_t \left[\frac{t}{\tau} + \frac{2}{\pi^2} \sum_{k=1}^{\infty} \frac{1 - \exp(-\pi^2 k^2 t/\tau)}{k^2} \right] \tag{14}$$

Fig. 3(b) presents a typical potential transient based on Eq. (14) [13]. As shown in this figure, R_{bulk} and R_t can be obtained from the initial potential rise and interpolation line of the potential after the $0.5t/\tau$ region, respectively. Interestingly, the intercept of the $V(t)/I_0$ axis corresponds to $R_t/3 + R_{bulk}$, which has a meaning similar to the ESR (R) described in Eq. (2), ESR $\approx R_t/3 + R_{bulk}$. From this relationship, Eq. (15) is obtained [2,3], i.e.,

$$R_{electrolyte} \approx \frac{R_t}{3} \tag{15}$$

This observation is discussed again in the section on a.c.-impedance analysis. In practical terms, the potential transient can be expressed in the time range between 0 and 0.3τ ($0 < t < 0.3\tau$), which produces [13]:

$$V(t) = \frac{2I_0R_t}{\pi} \left(\frac{t}{\tau} \right)^{0.5} \tag{16}$$

Next, Eqs. (11) and (16) are employed to obtain R_t from the two transient experiments.

For EIS, Eq. (7) should be used after inserting $j2\pi f$ in place of the s parameter [24–26]. Hence, Eq. (17) is obtained easily, namely:

$$Z(f) = \frac{R_t}{\sqrt{\tau 2\pi f j}} \coth[\sqrt{\tau 2\pi f j}] \tag{17}$$

From the separation of Eq. (17) into real and imaginary parts for the Nyquist plot, the real part of $Z(f)$ is given as:

$$Z_{real}(f) = \frac{R_t}{\sqrt{4\pi\tau f}} \frac{\sinh\sqrt{4\pi\tau f} - \sin\sqrt{4\pi\tau f}}{\cosh\sqrt{4\pi\tau f} - \cos\sqrt{4\pi\tau f}} \tag{18}$$

When the frequency (f) goes to zero, Eq. (19) is obtained [2,3], i.e.,

$$Z_{real} \approx \frac{R_t}{3} \tag{19}$$

From comparison between Eqs. (3) and (19), the ESR obtained in the TLM converges to $R_t/3$ when $R_{electrode}$ and R_{bulk} are disregarded. Hence, it is concluded that Eq. (15) also holds in EIS. The Nyquist plot of $Z(f)$ when $R_t = 1\ \Omega$ and $\tau = 1$ s is illustrated in Fig. 4(a). When f approaches a very low value (10^{-5} Hz), the real part of the impedance converges to 1/3. In the EIS result for real EDLC electrodes, however, distribution factors other than the surface roughness are affected by the composite electrodes, and pore-size

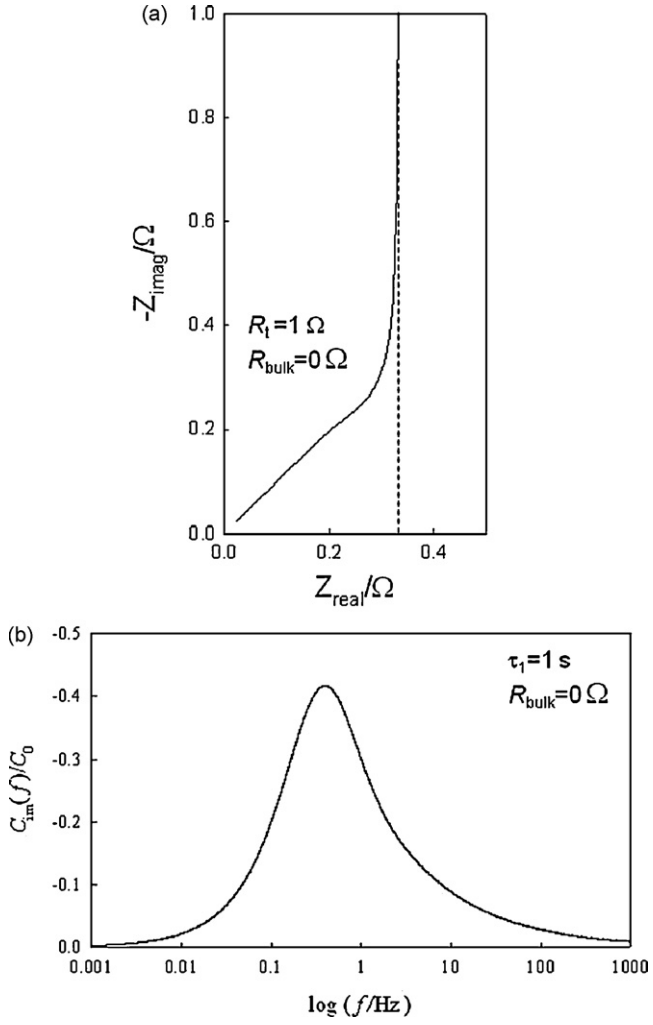

Fig. 4. (a) Typical Nyquist plot of $Z(f)$ when $R_{bulk} = 0\ \Omega$ and $R_t = 1\ \Omega$ and $\tau = 1$ s. Note that when f goes to very low value (10^{-5} Hz), real part of impedance converges to 1/3. (b) Typical curve of C_{im} *vs.* $\log f$ using graphical analysis in condition of $\tau = 1$ s and $R_{bulk} = 0\ \Omega$.

and length distribution most likely retard the appearance of a vertical line in the low-frequency region, thus making it difficult to estimate R_t by means of Eq. (19).

As reported by Jang et al. [8,9], imaginary capacitance analysis (ICA) has been proven suitable for the investigation of porous systems. Although the distributed factors addressed above exist in the electrodes, analysis of a porous system using ICA was found to be simple and easy. In the ICA, the imaginary part, ($C_{im}(f)$), of the complex capacitance, ($C(f)$), is given by:

$$C(f) = \frac{1}{2\pi f j Z(f)} \tag{20}$$

$$C_{im}(f) = -\frac{C_0}{\sqrt{4\pi\tau f}} \frac{\sinh\sqrt{4\pi\tau f} - \sin\sqrt{4\pi\tau f}}{\cosh\sqrt{4\pi\tau f} + \cos\sqrt{4\pi\tau f}} \tag{21}$$

In Fig. 4(b), the peak-shaped curve of C_{im} is presented using graphical analysis for the typical condition of $\tau = 1$ s and $R_{bulk} = 0\ \Omega$. Additionally, Eqs. (22) and (23) were obtained from this curve analysis [8,9].

$$C_0 = \frac{A}{0.682} \tag{22}$$

$$R_t = \frac{0.273}{f_p A} \tag{23}$$

Here, A and f_p are the peak area in the C_{im} curve obtained by numerical integration and peak frequency, respectively.

In summary, four transient equations based on CA, CP, ACI, and ICA are proposed to estimate the value of R_t in the theoretical section. The ESR considering $R_{electrode}$ and R_{bulk} in the TLM model can be expressed conclusively, as follows.

$$ESR = R_{electrode} + R_{bulk} + R_{electrolyte} \approx R_{electrode} + R_{bulk} + \frac{R_t}{3} \tag{24}$$

If other resistance components exist in the EDLC system, they should be added for the ESR calculation. This is discussed later.

4. Results and discussion

4.1. Characterization of carbon material

The direct template method was employed for easy and inexpensive preparation of mesoporous carbon [5–7]. It has been shown that carbon materials prepared using the direct template method exhibit improved EDLC performance due to their outstanding mesoporosity and good pore connectivity [17]. In our experiment, the meso-structure of the surfactant/silicate template is produced in advance within the solution phase. This template solution was reacted for several hours to enhance the growth of surfactant/silicate aggregates. After reaction of the template, a carbon precursor consisting of resorcinol–formaldehyde (RF) was added to the template solution. This composite, consisting of silicate + surfactant + RF, was polymerized, carbonized and etched using HF acid to produce mesoporous carbon. During the etching process, the silica remaining after carbonization was converted into mesopores in the carbon materials [17]. In particular, the reaction time of the surfactant/silicate template before the addition of the carbon precursor was varied from 2 to 16 h. During this reaction, the aggregates of surfactant/silicate converted into pores in the carbon became larger. Consequently, an increase of the carbon pore size was expected with increasing reaction time [20].

Fig. 5(a) shows the change in the pore-size distribution (PSD) of the carbon according to the reaction time. Additionally, Fig. 5(b) presents the change in the BET surface area (A_{BET}). For convenience, the carbon materials prepared with reaction times of 2, 5, 7 and 16 h are named C2, C5, C7 and C16, respectively. As can be seen,

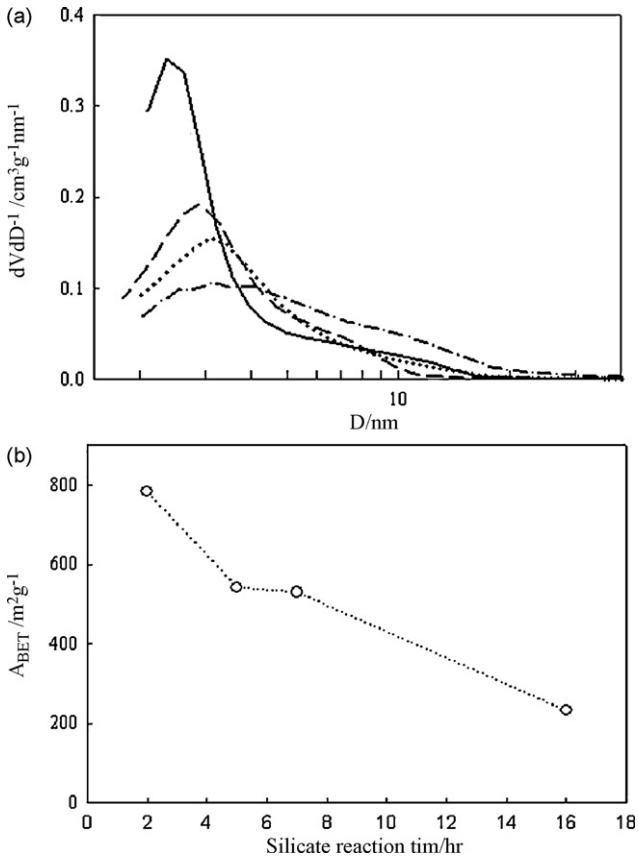

Fig. 5. (a) Change in pore-size distributions (PSD) of carbons according to reaction time. Solid line, dashed line, dotted line and dash-to-dot line are C2, C5, C7 and C16, respectively. (b) Change of BET surface area (A_{BET}).

the pore size of the carbon materials increases and the corresponding surface area decreases with increasing silicate reaction time. This trend is attributed to growth of the silicate/surfactant aggregates and to collapse of the pore structure. This gradual collapse of the pore structure with increasing silicate reaction time is currently under investigation using other physical analysis tools. SEM and TEM images of the carbon prepared with a reaction time of 2 h are shown in Fig. 6. Tubular morphology and wormhole-like pore morphology are observed and is characteristic of mesoporous silica produced by the surfactant template method [20]. Hence, the prepared carbon materials are suitable for EDLC electrodes because of their highly porous nature and good mesoporosity [5–7], and therefore EDLC electrodes were fabricated using these materials to verify the proposed transient equations. After the transient experiments, R_t and ESR values were obtained and compared, and the relationship between the pore structure and ESR was examined.

4.2. Various transient analyses using prepared carbon materials

Before carrying out transient experiments, the EDLC performance of the fabricated electrodes was investigated by means of cyclic voltammetry (CV). The capacitance *vs.* voltage profiles are shown in Fig. 7, and were obtained using CV at a scan rate of 5 mV s^{-1}. Here the capacitance is estimated by dividing the observed current by the scan rate employed in the CV experiment. As seen in the figure, a rectangular shape characteristic of EDLCs is observed, indicating that the prepared mesoporous carbons are suitable for use as EDLC electrodes materials. Since the capacitance of the EDLC electrodes is roughly proportional to surface area, the observed capacitance decreases in the order of C2 > C5 > C7 > C16, which is similar to the change in the surface area, as shown in

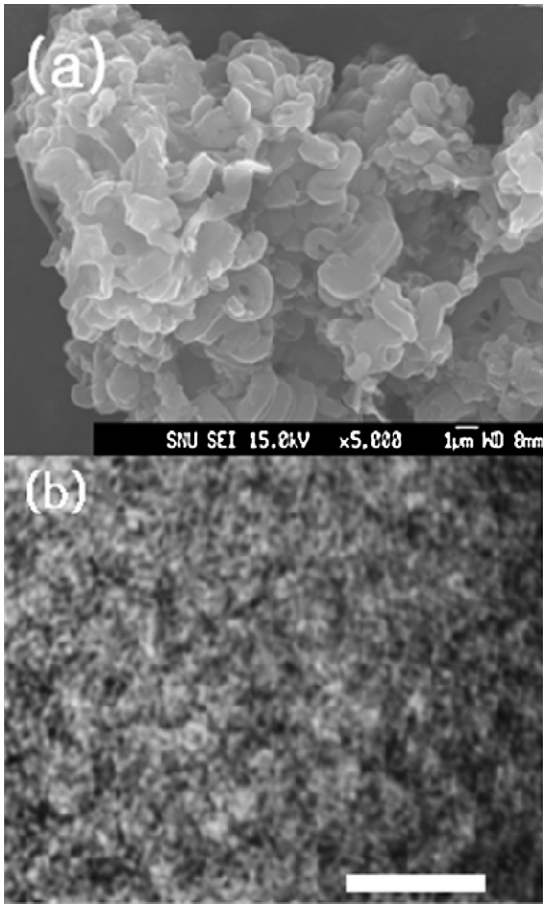

Fig. 6. (a) SEM and (b) TEM image of 2 h reaction carbon. White scale bar represents 50 nm in TEM image.

Fig. 5(b) [2,3]. A slight pseudo-capacitance induced by the charge-transfer reaction for quinine/hydroquinone is observed near 0.3 V *vs*. SCE, a characteristic that has generally been observed for carbon electrodes [27]. To avoid the effect of this pseudo-capacitive reaction on the transient signal, 0.5 V *vs*. SCE was selected as the base potential for the subsequent transient experiments.

EIS was conducted using an external sinusoidal voltage with a magnitude of 10 mV in the frequency region from 10^{-3} to 10^5 Hz after current stabilization at 0.5 V to within a few μA. From these results, the Nyquist plot for the carbon composite electrodes

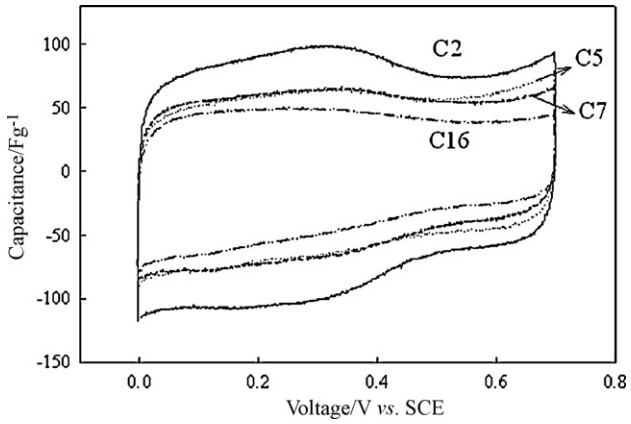

Fig. 7. Capacitance *vs*. voltage profiles obtained from cyclic voltammogram of EDLC electrodes fabricated by prepared carbon (scan rate = 5 mV s^{-1}). Carbon used is depicted within the graph.

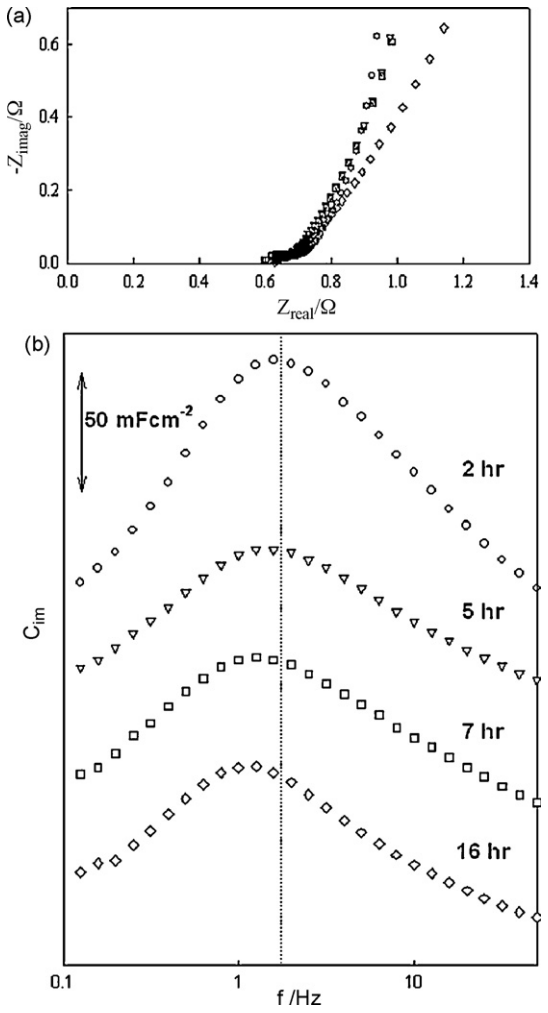

Fig. 8. (a) Nyquist plot from a.c.-impedance analysis measured at 0.5 V *vs*. SCE. (b) C_{im} *vs*. log *f* plot for carbon composite electrodes. Circle, inverse-triangle, rectangular and diamond symbols are C2, C5, C7 and C16 electrodes, respectively.

was obtained and is displayed in Fig. 8(a). All of the electrodes report almost the same intercept value on the Z_{real} axis of about 0.6 Ω, which is indicative of their identical EDLC cell structure. The $R_{electrodes}$ value of the porous carbon electrodes calculated from the measured electronic resistivity of the composite electrodes ($\rho_{electrode}$) is approximately 10 Ω cm, the apparent surface area ($A_{electrode}$) is 2 cm^2, and the electrode thickness ($t_{electrode}$) is about 25 μm. Using the relationship described in Appendix A, the calculated value of $R_{electrode}$ is 0.013 Ω. Similarly, R_{bulk} is estimated from the resistivity of the bulk electrolyte in 2.0 M H_2SO_4 (ρ_{bulk} = 1.47 Ω cm) as well as the gap between the working and reference electrodes (d = 0.58 cm). From the Nyquist plot, it is reported that the intercept value of the Z_{real} axis corresponds to the summation of R_{bulk} and $R_{electrodes}$, which describes the very fast frequency response of electron transport within the percolation network in the electrodes and electrolyte transport in the bulk solution [5,28]. Therefore, the expected intercept value of the Z_{real} axis should be 0.59 Ω ($R_{bulk} + R_{electrode}$), which perfectly coincides with the observed intercept point in Fig. 7(a). Interestingly, a semicircle (R_{semi}) of very small size (~0.1 Ω) appears after the Z_{real} intercept in the high-frequency range from 10^5 to 10^3 Hz, This may be related to phenomena similar to the slight pseudo-capacitive reactions on the electrode surface [29]. Although an ideal EDLC should completely utilize the electric double layer on the carbon surface, the capacitive contribution of the surface charge-transfer reaction originating

from the trace amount of surface functional groups is inevitable [2,29]. After this semicircle, a sloped line appears with decreasing frequency, which is related to the electrolyte transport in the pores. A vertical line follows the sloped line, which is similar to the Nyquist plot theoretically predicted using TLM, as shown in Fig. 4(a). From Eq. (19), one can roughly estimate the value of R_t from the intercept of Z_{real} obtained via the interpolation of the vertical line in the very low-frequency range. At first glance, an increase of R_t from C2 to C16 is observed qualitatively in Fig. 7(a). It is difficult, however, to calculate the exact value of R_t from the Nyquist plot because of other distributed elements such as the electrode surface roughness, pore-size distribution, and pore length distribution [11,12,30].

The EIS result was converted to ICA to measure R_t and τ. In Fig. 8(b), the profiles of C_{im} *vs.* log(f) are presented, and peak-shaped profiles characteristic of charge storage in a porous system are observed. Additionally, decreases of f_p and A are observed with increasing silicate reaction time, which is indicative of an increase in τ and decrease in C_0. From the measured values of f_p and A for each carbon electrode, C_0 and R_t were calculated using Eqs. (22) and (23), respectively. The results are listed in Table 1. Interestingly, the C_0 values of the individual carbon electrodes are similar to the specific capacitances in the cyclic voltammograms with consideration of the electrode weight (Fig. 6) for C2, 87 F g^{-1} in the ICA and 81 F g^{-1} in the CV. The change of R_t is discussed later.

Two other transient experiments (CA and CP) were conducted for the purpose of comparison with the ICA method. In Fig. 9, the result of the CA experiment is displayed. To acquire a clear transient signal, the surface charge of the electrodes was stabilized as follows. After several cycles of the CV experiment, a constant anodic current of 0.1 mA was applied from 0.7 to 0.5 V *vs.* SCE (CC (constant current) mode) and the potential was kept constant at 0.5 V until the measured current was stabilized to within a few μA (CV (constant voltage) mode). After stabilization of the current, a potential step with a magnitude of 10 mV was applied to the electrodes and the resulting current transient was recorded every 10 ms. For convenient utilization of Eq. (11), the measured current transient ($I(t)$) was plotted against $(\tau/t)^{0.5}$. Here the measured τ obtained from ICA was used for convenience. R_t was estimated using the tangent line from the zero point; this procedure is shown in Fig. 8(b). A distinct decrease of the slope from electrodes C2 to C16 is clearly observed, reflecting the increase of R_t. The estimated values of R_t are listed in Table 1.

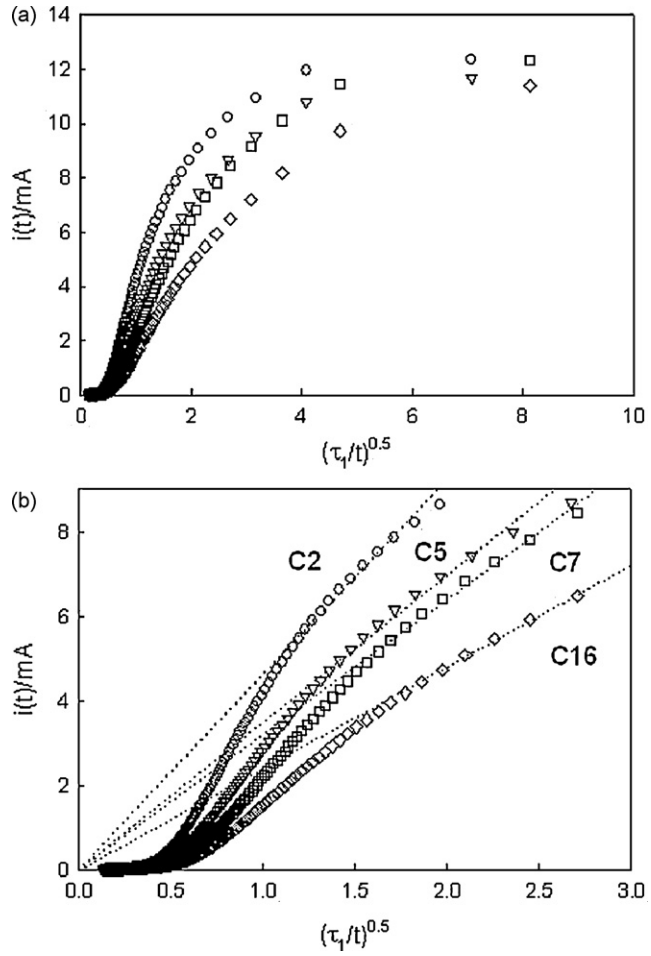

Fig. 9. (a) Measured current transient ($I(t)$) plotted against $(\tau/t)^{0.5}$. Here, circle, inverse-triangle, rectangular and diamond symbols are C2, C5, C7 and C16 electrodes, respectively. (b) Magnification in region from 0 to $0.3(\tau/t)^{0.5}$. Tangent line from zero point added as dotted line.

For the CP measurement, a current step with a magnitude of 10 mA was applied to the electrodes after the same CC–CV stabilization process. Fig. 10(a) shows the resulting V_{meas} transient signal *vs.* time (t) measured every 10 ms. As expected, based on Fig. 3(b), an initial rise of the potential and subsequent straight line are observed in Fig. 10(a). Estimation of R_{bulk} seems to be difficult, however, because it can depend on the sampling time and the initial potential rise as it converges to R_{bulk} as the sampling time is decreased. After extraction of the base potential (0.5 V *vs.* SCE) from V_{meas}, the potential transient ($V(t)$) was obtained, $V(t) = V_{meas} - 0.5$. For easy calculation of R_t, plots of $V(t)$ against $(t/\tau)^{0.5}$ are shown in Fig. 10(b). Note that the time (t) from 0 to 0.3τ should be utilized for estimation with Eq. (16). When $t = 0.3\tau$, $(t/\tau)^{0.5} = 0.55$. Hence, the range of $(t/\tau)^{0.5}$ from the initial rise to 0.55 was used for the calculation of R_t. In Table 1, R_t obtained from CP is listed to facilitate comparison. Interestingly, the estimated values of R_t are similar, irrespective of the measurement method.

In the three transient measurements, R_t increases with increasing silicate reaction time. When considering the definition ($R_t = R_p/N_p$), the observed increase in R_t is probably due to a decrease in the number of pores (N_p) or an increase in the electrolyte resistance within each pore (R_p). First, a decrease of N_p may have been caused by a decrease in the surface area with increasing reaction time. Additionally, it is well-known that R_p is proportional to the square of the pore diameter (D_p) and inversely proportional to the pore length (l_p); $R_p \propto l_p D_p^{-2}$ [2]. Since D_p increases with increasing silicate reaction time (Fig. 5(a)), an increase of R_p may be due to an increase of l_p, which is related to the gradual collapse of the pores with increasing silicate reaction time. In our preliminary experiment, it was confirmed that the collapse of the pore structure became more severe from C2 to C16 based on the results of small angle X-ray diffraction experiments. Hence, it can be concluded that various factors pertaining to the pore structure, such as the pore size, pore length and number of pores, can act together to influence R_t.

According to the results of the three measurements, the ESR was estimated from its definition, as follows:

$$\mathrm{ESR} = \sum_k R_k = R_{electrode} + R_{bulk} + R_{semi} + R_{electrolyte} \approx R_{electrode} + R_{bulk} + R_{semi} + \frac{R_t}{3} \quad (25)$$

where $R_{electrode}$, R_{bulk} and R_{semi} are 0.58, 0.01, and 0.1 Ω for convenience, respectively. After normalization using the apparent electrode area (ca. 2 cm^2), the calculated value of the ESR is listed in Table 1. Interestingly, the estimated value of the ESR approximately coincides with Z_{real} when f goes to zero in the Nyquist plot, demonstrating the consistency of the three transient measurements of the ESR employed herein. The observed ESR value of the carbon

Table 1
Results of transient experiment with change of carbon.

Carbon	f_p/Hz	A/F	τ/s	C_0/F cm^{-2}	R_t/Ω cm^2			ESR[a]/Ω cm^2		
					ICA	CA	CP	ICA	CA	CP
C2	1.6	0.295	0.25	0.213	1.16	1.44	1.20	1.78	1.88	1.80
C5	1.6	0.195	0.25	0.143	1.76	1.92	1.72	1.98	2.04	1.98
C7	1.2	0.190	0.33	0.140	2.36	2.12	1.84	2.18	2.10	2.02
C16	1.2	0.185	0.33	0.135	2.92	3.08	3.08	2.22	2.36	2.42

[a] ESR was estimated from summation of $R_{electrode}$, R_{bulk}, R_{semi} and $R_{electrolyte}$ (ESR = $R_{electrode} + R_{bulk} + R_{semi} + R_{electrolyte} = R_{electrode} + R_{bulk} + R_{semi} + R_t/3$).

electrode prepared with a reaction time of 2 h was 1.2–1.8 Ω cm^2, which is comparable with that of the ordered mesoporous carbon electrode prepared using the MCM-48 (1.50 Ω cm^2) HMS template (2.84 Ω cm^2) [5,6]. The observed high-rate performance of the carbon electrode prepared with a reaction time of 2 h is most likely due to the merits of the templating method for preparation of the mesoporous carbon, viz. its resulting high mesoporosity and good pore connectivity [16]. Furthermore, the present direct templating method is simple and inexpensive when compared with preparation of porous carbon using a solid ordered mesoporous silica template [17].

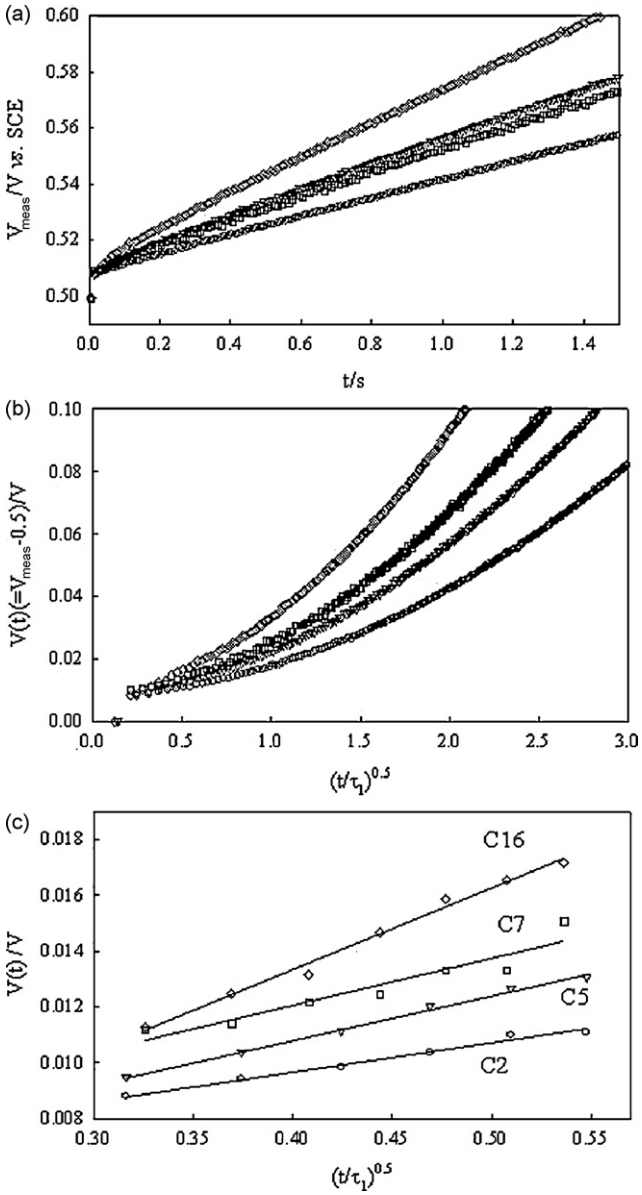

Fig. 10. (a) Measured V_{meas} transient signal *vs.* time (t) measured every 10 ms. (b) Profiles of potential transient ($V(t)$) *vs.* $(t/\tau)^{0.5}$. $V(t)$ obtained by extraction of base potential 0.5 V; $V(t) = V_{meas} - 0.5$. (c) Profiles of $V(t)$ *vs.* $(t/\tau)^{0.5}$ in time range of $0 < t < 0.3\tau$. Circle, inverse-triangle, rectangular and diamond symbols are C2, C5, C7 and C16 electrodes, respectively.

5. Conclusions

For ESR estimation in EDLC electrodes, transient equations based on two equivalent circuit models (simplest model and transmission line one) have been established. In order to verify the proposed equations, mesoporous carbon materials prepared by direct templating method are utilized as EDLC electrodes and transient experiments are conducted using them. The ESRs are acquired using the proposed equations and are then compared. The following points summarize the findings.

(i) For the simplest equivalent circuit model based on series connection of resistance and capacitance, the well-known simple transient equations are given.
(ii) For the transmission line model, equations for the three transient experiments (chronoamperometry, chronopotentiometry, and a.c.-impedance) are proposed. From the obtained equations, it is shown that one-third of the total electrolyte resistance encompassing the ionic transport within the pores contributes to the ESR.
(iii) After preparation of mesoporous carbons with different pore structures, EDLC electrodes have been fabricated and applied to transient experiments. From the analysis using the proposed equations, consistent and similar results of ESR are obtained, irrespective of the transient methods.
(iv) Due to the merit of the template method in preparing mesoporous carbon, the carbon electrode prepared with a reaction time of 2 h exhibits an improved rate performance.

Acknowledgements

This research was supported by a grant from the Fundamental R&D Program for Core Technology of Materials funded by the Ministry of Knowledge Economy, Republic of Korea (Project number: TS097-17-1).

Appendix A. Nomenclature

A_{BET}	BET surface area (m^2 g^{-1})
$A_{electrode}$	apparent electrode surface area (cm^2)
V_{pore}	pore volume (cm^3 g^{-1})
d	electrodes gap between working and reference (cm)
D_p	pore diameter (nm)
l_p	pore length (μm)
l	length from the entrance of pore (mm)
y	dimensionless parameter of pore length ($y = l/l_p$)
I_0	applied current during chronopotentiometry (mA)

$I(t)$ resulting current transient during chronoamperometry (mA)
V_0 applied potential during chronoamperometry (mV)
V_{meas} measured voltage signal in chronopotentiometry (V)
V_{base} base potential where transient experiment is conducted (V)
$V(t)$ resulting potential transient ($V(t) = V_{meas} - V_{base}$) (V)
m number of pores in one particle
n particle number of porous materials
N_p total pore number of electrodes ($N_p = m \times n$)
$R_{electrode}$ electrical resistance of electrode ($R_{electrode} = \rho_{electrode} t_{electrode}/A_{electrode}$) ($\Omega$)
R_{bulk} bulk electrolyte resistance ($R_{bulk} = \rho_{bulk} d/A_{electrode}$) ($\Omega$)
R_{semi} resistance of semicircle in Nyquist plot (Ω)
$R_{electrolyte}$ total electrolyte resistance of electrode (Ω)
R equivalent series resistance (ESR) ($R = R_{electrode} + R_{semi} + R_{bulk} + R_{electrolyte}$) ($\Omega$)
r electrolyte resistance per unit pore length ($\Omega\,cm^{-1}$)
R_p electrolyte resistance within one pore ($R_p = r \times l_p$) (Ω)
R_t total electrolyte resistance in pores ($R_t = R_p/N_p$) (Ω)
$t_{electrode}$ electrode thickness (μm)
c double-layer capacitance per unit pore area ($F\,cm^{-2}$)
C_p double-layer capacitance in one pore ($C_p = C_A \pi D_p l_p$) (F)
C_0 total capacitance of electrode ($C_0 = N_p C_p$) (F)
s parameter in Laplace domain
f frequency (Hz)
Z_p impedance of one pore (Ω)
Z overall impedance of total pores (Ω)
C complex capacitance (F)
C_{im} imaginary capacitance (F)
A peak area in imaginary capacitance plot (F)
f_p peak frequency in imaginary capacitance plot (Hz)

Greek letters

τ time constant for pores ($\tau = R_p C_p = R_t C_0$) (s)
$\rho_{electrode}$ electronic resistivity of composite electrodes (Ω cm)
ρ_{bulk} resistivity of bulk electrolyte in 2.0 M H_2SO_4 (Ω cm)

References

[1] H. Shi, Electrochim. Acta 41 (1996) 1633.
[2] B.E. Conway, Electrochemical Supercapacitors, Kluwer Academic/Plenum Publisher, 1999.
[3] R. Kötz, M. Carlen, Electrochim. Acta 45 (2000) 2483.
[4] S.-R. Hwang, H. Teng, J. Electrochem. Soc. 149 (2002) A591.
[5] S. Yoon, J. Lee, T. Hyeon, S.M. Oh, J. Electrochem. Soc. 147 (2000) 2507.
[6] J. Lee, S. Yoon, S.M. Oh, T. Hyeon, Adv. Mater. 12 (2000) 359.
[7] J. Lee, S. Yoon, S.M. Oh, T. Hyeon, Chem. Commun. (1999) 2177.
[8] J.H. Jang, S.M. Oh, J. Electrochem. Soc. 151 (2004) A571.
[9] S. Yoon, J.H. Jong, B.H. Ka, S.M. Oh, Electrochim. Acta 50 (2005) 2255–2262.
[10] R. de Levie, in: P. Delahay (Ed.), Advances in Electrochemistry and Electrochemical Engineering, vol. VI, John Wiley & Sons, New York, 1967, p. 329.
[11] H.-K. Song, Y.-H. Jung, K.-H. Lee, L.H. Dao, Electrochim. Acta 44 (1999) 3513.
[12] H.-K. Song, H.-Y. Hwang, K.-H. Lee, L.H. Dao, Electrochim. Acta 45 (2000) 2241.
[13] F.A. Posey, T. Morozumi, J. Electrochem. Soc. 113 (1966) 176.
[14] O. Lanzi, U. Landau, J. Electrochem. Soc. 137 (1990) 585.
[15] S.H. Joo, S.J. Choi, I. Oh, J. Kwak, I. Liu, O. Terasaki, R. Ryoo, Nature 412 (2001) 169.
[16] E. Frackowiak, F. Beguin, Carbon 40 (2002) 1775.
[17] S. Yoon, S.M. Oh, C. Lee, Mater. Res. Bull. 44 (2009) 1663.
[18] D. Zhao, J. Feng, Q. Huo, N. Melosh, G.H. Fredrickson, G.H. Chimelka, G.D. Stucky, Science 279 (1998) 548.
[19] J.Y. Ying, C.P. Mehnert, M.S. Wong, Angew. Chem. Int. Ed. 38 (1999) 56.
[20] J. Xu, Z. Luan, H. He, W. Zhou, L. Kevan, Chem. Mater. 10 (1998) 3690.
[21] C.T. Kresege, M.E. Leonowicz, W.J. Roth, J.C. Vartuli, J.S. Beck, Nature 359 (1992) 710.
[22] R.W. Pekala, D.W. Schaefer, Macromolecules 26 (1993) 5487.
[23] A.J. Bard, L.R. Fulkner, Electrochemical Methods: Fundamentals and Applications, John Wiley & Sons, New York, 1988, p. 15.
[24] D.D. Macdonald, M. Urquidi-Macdonald, J. Electrochem. Soc. 132 (1985) 2316.
[25] M. Urquidi-Macdonald, S. Real, D.D. Macdonald, J. Electrochem. Soc. 133 (1986) 2018.
[26] D.D. Macdonald, Transient Techniques in Electrochemistry, Plenum Press, New York/London, 1977.
[27] K. Kinishita, Carbon: Electrochemical and Physicochemical Properties, John Wiley & Sons, New York, 1988.
[28] B.-L. He, B. Dong, H.-L. Li, Electrochem. Commun. 9 (2007) 425.
[29] T. Osaka, M. Datta, Energy Storage Systems for Electronics, Gordon and Breach Science Publisher, 2000, pp. 528–530.
[30] H. Keiser, K.D. Beccu, M.A. Gutjahr, Electrochim. Acta 21 (1976) 539.